INSTITUTE OF PHYSICS PUBLISHING PLASMA PHYSICS AND CONTROLLED FUSION

Plasma Phys. Control. Fusion **45** (2003) 89–103 PII: S0741-3335(03)40079-1

Spectroscopic observation of Si I- and Si II-emission lines in the boundary of TEXTOR and comparison with kinetic calculations

A Huber[1], I Beigman[2], D Borodin[1,2], Ph Mertens[1], V Philipps[1], A Pospieszczyk[1], U Samm[1], B Schweer[1], G Sergienko[1,3] and L Vainshtein[2]

[1] Institut für Plasmaphysik, Forschungszentrum Jülich GmbH, EURATOM Association, Trilateral Euregio Cluster, 52425 Jülich, Germany
[2] Lebedev Institute, Russian Academy of Sciences, 119991 Leninski pr. 53, Moscow, Russia
[3] Institute of High Temperatures, Russian Academy of Sciences, Moscow, Russia

Received 1 July 2002, in final form 19 November 2002
Published 31 December 2002
Online at stacks.iop.org/PPCF/45/89

Abstract

Measurements of Si I- and Si II-emission lines were performed in the front of a test limiter under two different conditions: (i) silicon is sputtered from a silicon layer deposited on a graphite test limiter, (ii) silane is puffed into the plasma through a gas inlet in the limiter head, setting Si-atoms free from the dissociation of SiD_4 molecules. It was shown that the relative intensities of the emission lines within the multiplets are in good agreement with theoretical data calculated in the SL-coupling scheme. The values for 'ionization per photon' were calculated for the electron temperature range below 100 eV using the GKU kinetic code and compared with measured ones. The measured and theoretical values for the Si II-emission lines are in reasonable agreement within a deviation of 30%. It was found that experimentally measured values for Si I lines match the calculated ones only when a LTE-population of $3p^2$ SL terms (^3P, ^1D and ^1S) is assumed.

1. Introduction

The control of plasma purity and power deposition on limiter or divertor components is a serious problem in fusion devices. Interactions of the plasma with the walls lead to particle release by various mechanisms and the amount of impurities in the plasma core limits the performance of the device.

One efficient way to control the impurities in the plasma is by coating the entire first wall with a thin layer of amorphous silicon (siliconization) [1]. It has been successfully applied at TEXTOR and other devices and improved the plasma performance. Carbon and oxygen fluxes are significantly reduced after the coating with silicon and the density limit is strongly enhanced [2–4]. Moreover, silicon atoms are good oxygen getter and practically

non-recycling. Although silicon is a medium-Z material, the radiation due to silicon is located at the plasma periphery, thus providing radiation cooling at the plasma edge by which heat loads on the limiter or divertor can be reduced and controlled [2]. In the TEXTOR tokamak, siliconization has led not only to a highly radiative mantle formation but also to improved energy confinement (RI-mode) maintaining energy confinement significantly above the ITER 89P L-mode empirical scaling relation [1,5].

Additionally, silicon is widely used as dopant to a graphite matrix, a technique which can significantly reduce the chemical erosion of graphite through molecule formation [6–8]. Furthermore, SiC is also an attractive candidate for special applications as structural (inside the blanket) or even wall material in a fusion reactor, because of its low radioactivity in connection with good mechanical and isolating conditions [9].

Thus, the possible use of Si under fusion conditions calls for reliable measurements of eroded silicon fluxes by spectroscopic means. These fluxes can be determined by passive spectroscopy, provided the 'ionization per photon' values (so-called *S/XB* values) are available. In this case, the particle flux can be calculated from the measured line intensity as described in the literature (see, e.g. [10–12]), on the condition that the spatial dependence of the rate coefficients is weak in the region of interest, which usually means that they should not vary appreciably with the electron temperature T_e:

$$\Gamma = I \frac{S}{XB}, \tag{1}$$

where I (photons s^{-1}) is the total intensity of the Si I- or Si II-emission lines, S and X are rate coefficients for ionization and excitation respectively, and B is the branching ratio for the transition of interest. *S/XB* values are thus required for selected spectrum lines. In this work, calculations of *S/XB* values for different Si I- and Si II-emission lines were performed using the GKU kinetic code (see section 3.3) and the results were compared with experimental data.

2. Experimental set-up

The experiments have been performed in the tokamak TEXTOR which has a major radius $R = 1.75$ m and a minor radius $a = 0.46$ m. TEXTOR was operated with a toroidal magnetic field $B_T = 2.25$ T and a plasma current of $I_p = 350$ kA. The line averaged central electron density was varied between $\bar{n}_e = 2.5 \times 10^{19}\,m^{-3}$ and $\bar{n}_e = 6 \times 10^{19}\,m^{-3}$. Additional heating was provided by a neutral beam injector (NBI) injecting tangentially in the co-direction of the current with a power of 1.3–1.5 MW.

The measurements have been performed in two experimental campaigns: the first campaign was carried out in series of discharges with freshly siliconized walls. The vessel walls had been siliconized using a standard RF assisted DC plasma with a mixture of 80% He and 20% SiH_4 or SiD_4 as precursor gas [1]. Si films of about 120–150 nm are deposited rather uniformly over the entire wall. Special test limiters were also coated *in situ* [3] and the Si-release was observed spectroscopically during the experiments.

In a second campaign, silicon was injected as silane through an equivalent test limiter. The test limiter had dimensions of 12 cm × 8 cm and a spherical shape with a radius of 7 cm. It was inserted from the top of the torus into the edge plasma through a limiter-lock as shown in figure 1 [13] to the position of the last closed flux surface (LCFS) at $r = 0.46$ m or slightly outside the confined plasma at $r = 0.465$ m. For gas injection, a hole was drilled through the limiter at a toroidal position 20 mm from the centre. The hole was located on the ion drift side of the limiter and the spectral lines have been observed at the point of the gas injection via a tangential view in poloidal direction.

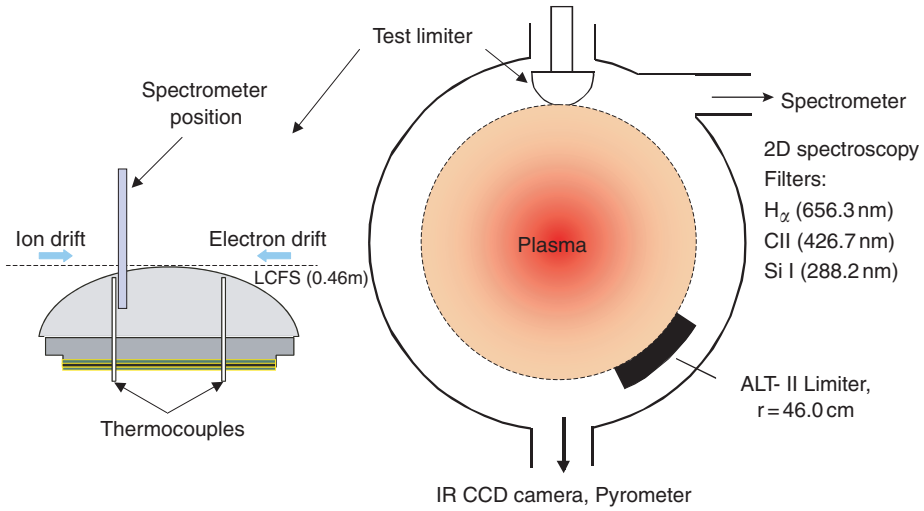

Figure 1. Experimental set-up of the limiter lock at TEXTOR with the spectroscopic observation system.

The silicon release from this limiter was studied using an image intensified CCD camera coupled to a spectrometer (Ebert type, $f = 0.5$ m), the entrance slit of which was focussed at a toroidal position 20 mm from the centre at the ion drift side. This position is near the spot of the highest power load. The radial intensity distribution of the impurity line emission was measured by an additional CCD camera equipped with interference filters with a bandwidth of 1.5 nm for the respective impurity line radiation (Si I (288.1 nm), D_α (656.1 nm)). The power deposition on the limiter surface was measured with a pyrometer and a CCD camera with an infrared edge filter (transmission wavelength from 850 nm). Additionally, the bulk temperature of each limiter side was monitored with thermocouples positioned 7 mm behind the surface near the location of the highest power load. Edge electron temperature and density profiles were measured at the equatorial plane by means of a thermal He-beam diagnostics [14].

3. Collisional-radiative model

3.1. Kinetic calculations

Kinetic calculations were done by the code GKU (for short outline see [15]). It gives the data for the level populations, intensities of the selected lines and *S/XB* factors. Two modes non-stationary (NS) and quasi-stationary (QS) are possible (see below). The atomic data-base (ADB) for the transitions between the levels considered was calculated by the code ATOM. If any atomic characteristic is absent in the ADB, it was calculated by the code using a set of formulae ('Bates-Damgaard' for oscillator strengths, semiclassical excitation and classical ionization formulae [16]).

Code ATOM calculates atomic characteristics such as transition probabilities and rate coefficients. It is based on the one-electron, semi-empirical wave functions without configuration interaction. For the collisional characteristics, Coulomb-Born-exchange approximation (CB) with K-matrix method for the channel interaction and normalization is used. For ionization cross-sections, besides the direct ionization from the outer shell, the contributions from the innershell ionization and excitation of autoionization levels are included. For more details see [17].

Final results are reconsidered if some experimental data or data obtained by such methods as convergent close-coupling (CCC) or R-matrix are available.

3.2. Atomic data

SL-coupling[4] was assumed in the collisional-radiative models of Si I and Si II. Additional calculations in the intermediate coupling scheme gave results reasonably close to SL-coupling. The states $3s^2 3p^2$, $3s^2 3p3d$, $3s^2 3p4l$, (all SL terms) are included in the Si I model, and the states $3s^2 3p$, $3s^2 3d$, $3s^2 nl$, $3 < n = 7, l = 4$ are included in the Si II model. The fine structure was not considered in most calculations. This means that fine structure J-levels are assumed to be populated according to the statistical weights $2J + 1$. The experimental results discussed below (section 4.2) prove that this assumption is indeed justified.

Radiative transition probabilities calculated by ATOM for most transitions are in agreement with data from compilation [18]. Only for two transitions, namely 3p–3d and 3d–4f, there is an essential difference, which can be explained by the configuration interaction. The values for transition probabilities from [18] were used for these two transitions. (See also additional information concerning configuration interaction for Si II in [19].) For ionization cross-sections, there are large contributions of ionization from the inner shell $3s^2$ and excitation of autoionizing levels 3s3pnl. The cross-sections for Si I and Si II obtained are in reasonable agreement with the recommended data from [20,21] and experimental data [22,23] (figure 2). Excitation cross-sections obtained by the KM method with 406 channels for Si I and 120 channels for Si II were used. For the 3p–3d and 3d–4f transitions, we introduced the correction factor A([18])/A([17]). Since the exchange excitation is not significant, this factor takes into account the configuration interaction effectively.

3.3. S/XB factors

The *S/XB* factor is used in many papers (see e.g. [24–26] and the review paper [12]). We use the quasi-stationary (QS) approach to the problem: and consider Si II ions in the boundary plasma at fixed values of the electron temperature T_e and density n_e. In this case, the number of photons per ion at a wavelength λ is [12,27]

$$q_\lambda = \frac{W_\lambda}{W_i} \tag{2}$$

where W_λ is the excitation rate for the selected line, obtained from solution of the stationary balance equations and $W_i = n_e \langle \sigma_i v \rangle$ is the ionization rate of the ion. W_λ / n_e and W_i / n_e are weak function of n_e and depend rather strongly on T_e. However, their ratio W_λ / W_i is independent of n_e for the cases considered in this paper and depends only weakly on T_e. This justifies the use of the QS approach. The usually used ionization per photon factor (*S/XB*), which allows to convert the photon to particle fluxes, corresponds to $1/q$. The factor q is more convenient since it is additive (over spectral lines) and small values of q correspond to week (insignificant) lines. Nevertheless, we give below values for more customary *S/XB* factors.

In this work, we consider the following Si II-emission lines at 412.9 nm (sum over multiplet lines 412.8054 and 413.0894 nm), 635.9 nm (sum over multiplet lines 634.711 and 637.137 nm), 596.8 nm (sum over multiplet lines 595.756 and 597.893 nm) and 504.8 nm (sum over multiplet lines 504.1024 and 505.5984 nm), corresponding to the transitions 3d–4f, 4s–4p, 4p–5s and 4p–4d, respectively. We also observe the following Si I-emission

[4] We preferably use the non-standard designation 'SL'- in place of 'LS'-coupling since the formulae for the transition amplitude are more natural and symmetrical. Calculations of this paper are based on the SL-coupling.

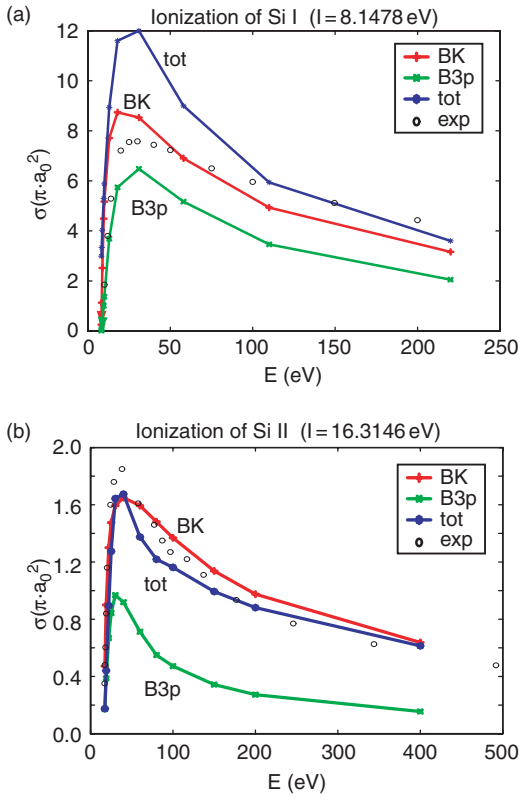

Figure 2. Ionization cross-section for Si I and Si II: 'BK' data from [20]; 'B3p' is the ionization from 3p shell calculated by ATOM-code; 'tot' is the total cross-section calculated by ATOM-code; 'exp' are experimental data [22, 23].

lines: 251.7 nm (transition $3p^2(^3P)$–$4s(^3P)$, sum over multiplet lines 250.6897, 251.4316, 251.6112, 251.9202, 252.4108 and 252.8508 nm), 288.1577 nm (transition $3p^2(^1D)$–$4s(^1P)$) and 390.552 nm (transition $3p^2(^1S)$–$4s(^1P)$). We took special care to use lines of different spin systems, in order to investigate the metastable states populations properly.

Figure 3 displays the level diagram of Si I (*a*) and Si II (*b*). It shows the strongest transitions including the lines observed in the experiment. In table 1, *S/XB*-factors for these lines (multiplets) are given for several values of T_e and n_e. For the Si II-emission lines, there is a significant dependence on T_e, but a somewhat less significant dependence on n_e. In the case of Si I, one sees a significant temperature dependence of the *S/XB* values for temperature below about 20 eV. Also the dependence on electron density is weak: the maximal deviation between *S/XB* values for the electron density range (2–8) $\times\ 10^{18}\ m^{-3}$ is smaller than 15%.

Figure 4(*a*) shows an example of *S/XB* ratios for Si II-emission lines for an electron density of $n_e = 2 \times 10^{18}\ m^{-3}$. The strongest lines are the Si II-emission lines at 635.9 nm (sum over multiplet lines 634.711 and 637.137 nm) corresponding to the transition $3s^2(^2S)4s$–$3s^2(^2P)4p$ for which *S/XB* = 2–6 holds. Also the lines at 412.9 and 504.8 nm can be recommended for silicon flux measurements. Approximate calculation of *S/XB* ratio for the line at 596.8 nm using the Regemorter formula [28] for excitation rate give result of a factor of two larger. This has led to an overestimation of silicon fluxes in [2, 29].

Figure 4(*b*) shows the *S/XB* ratio for Si I-emission lines at $n_e = 2 \times 10^{18}\ m^{-3}$. These calculation were performed using the GKU kinetic code based on the assumption of a

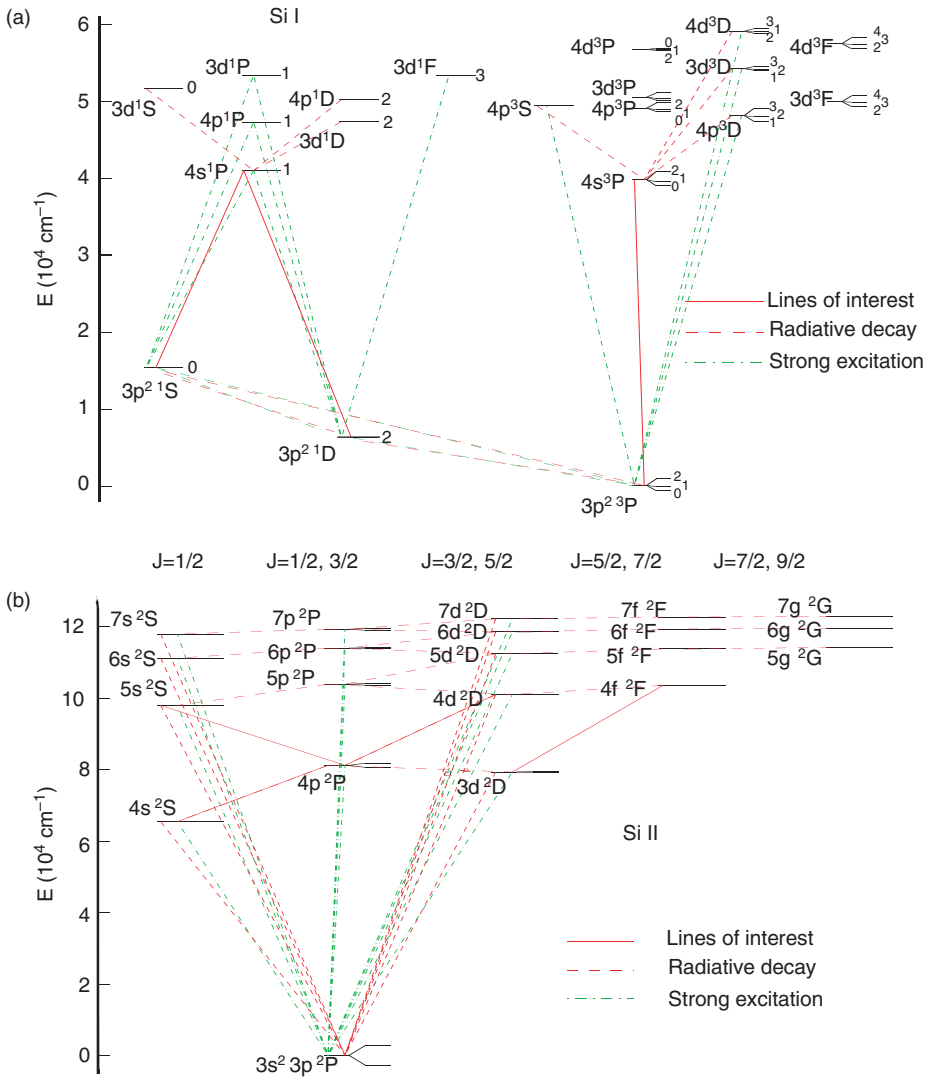

Figure 3. Level diagrams of the most important Si I (*a*) and Si II (*b*) states.

thermodynamical population of the $3p^2$ SL terms (^{3}P, ^{1}D and ^{1}S). This assumption will be explained in more detail in chapter 4.3. For silicon flux measurements, Si I-emission lines at 251.7 nm (a strong emission line with $S/XB = 7.0$ for $T_e = 40$ eV) and 288.155 nm (a strong emission line with $S/XB = 13.0$ for $T_e = 40$ eV) seem to be the preferred choice. The first one ($\lambda = 251.7$ nm) was used for laser-induced fluorescence (LIF) as well [30,31]. A disadvantage for the use of the Si I lines might lie in the accessibility in the UV region.

4. Comparison of the theoretical and experimental data

4.1. Experiments with siliconized walls

The measurements were made in a series of discharges under constant plasma conditions. Figure 5 shows as an example time traces of some central and local plasma parameters for

Table 1. Ionization per photon (T_e in eV, n_e in 10^{18} m^{-3}) for Si II- and Si I-emission lines.

		Si II				Si I $3p^2$–3p4s		
		3d–4f	4s–4p	4p–5s	4p–4d	^{3}P–^{3}P	^{1}D–^{1}P	^{1}S–^{1}P
T_e	n_e	412.9 nm	635.9 nm	596.8 nm	504.8 nm	251.7 nm	288.16 nm	390.55 nm
10	2	6.0	2.2	50.8	8.8	4.2	8.9	150.0
20	2	10.0	3.6	76.1	13.3	6.1	11.0	190.0
50	2	15.9	5.1	98.0	17.3	7.3	13.0	210.0
70	2	18.0	5.5	100.9	18.1	7.4	13.0	210.0
100	2	20.0	5.8	101.9	18.5	7.5	13.0	210.0
10	4	5.9	2.4	56.1	8.7	4.6	9.6	160.0
20	4	9.6	3.8	83.6	13.0	6.6	12.0	200.0
50	4	15.0	5.4	106.9	17.0	7.7	14.0	220.0
70	4	16.9	5.9	109.8	17.9	7.8	14.0	220.0
100	4	18.8	6.2	110.2	18.3	7.8	14.0	230.0
10	8	5.9	2.7	60.1	8.5	5.1	11.0	170.0
20	8	9.4	4.3	89.4	12.9	7.2	13.0	220.0
50	8	14.3	6.1	113.3	16.9	8.3	15.0	240.0
70	8	16.0	6.5	116.4	17.7	8.3	15.0	240.0
100	8	17.6	6.8	116.5	18.1	8.2	15.0	240.0

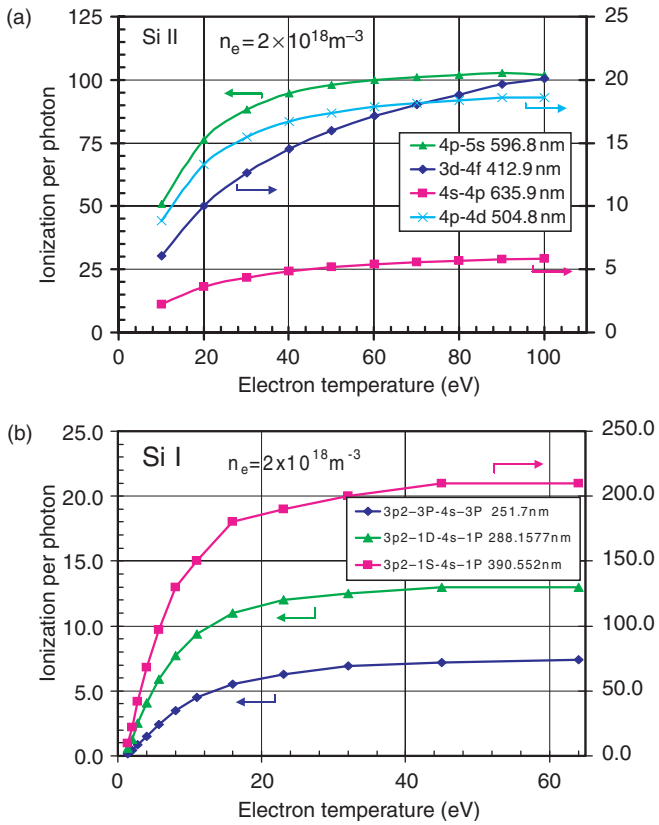

Figure 4. Ionization events per photon for several Si I- and Si II-emissions lines for electron density of 2.0×10^{18} m^{-3}.

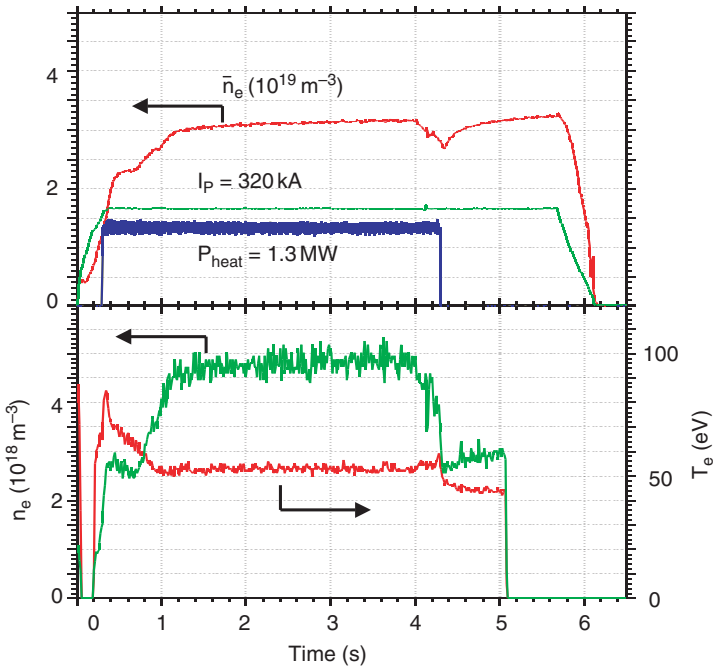

Figure 5. Time evolution of the central and local plasma parameter during experiments with freshly siliconized wall.

discharges with additional NBI heating of 1.3 MW. Edge electron temperature and density profiles were measured at the equatorial plane by means of He-beam diagnostics [14]. At the radial position of the test limiter the local T_e was about 53 eV and the local $n_e = 4.7 \times 10^{18}$ m^{-3} during the stationary phase of discharge.

Figure 6 shows the tangential view of the CCD camera directed to the test limiter in the light of Si I-emission line with a spatial resolution of about 0.5 mm. Silicon is eroded mainly by physical sputtering [3, 31]. The toroidal axis is oriented horizontally and the vertical axis refers to the radial direction (LCFS at $y = 0$, negative values corresponds to the scrape-off layer). The left (electron drift) side of the limiter is for this limiter radius shadowed by the main toroidal ALT II limiter due to a short connection length of 1.5 m. The intensity decrease exponentially with radius with a decay length of about 5–6 mm. The velocity distribution of sputtered silicon atoms was measured be means of laser-induced fluorescence in front of a SiC-limiter [31] and can be fitted by a Thompson distribution functions with a binding energy of $U_s = 4.8$ eV (the computed value is 4.7 eV [32]). Under the assumption of a Thompson velocity distribution function, the penetration depth can be calculated by

$$l = \frac{\bar{\upsilon}}{n_e \langle \sigma \upsilon \rangle_i}, \tag{3}$$

where $\bar{\upsilon}$ is an average velocity for the atoms, n_e is the electron density and $\langle \sigma \upsilon \rangle_i$ the rate coefficient for ionization by electron impact. The calculated penetration depth is about 5–7 mm and corresponds well with measured one.

Figure 7 shows Si II-emission spectra in four wavelength ranges in front of the test limiter:

(a) Wavelength range 410–436 nm with Si II-emission lines at 412.8054 and 413.0894 nm. These lines corresponds to the transition $3s^2(^2P)3d$–$3s^2(^2F)4f$. Due to presence of the D_γ-emission line and the large brightness of Si II lines, this spectral region is

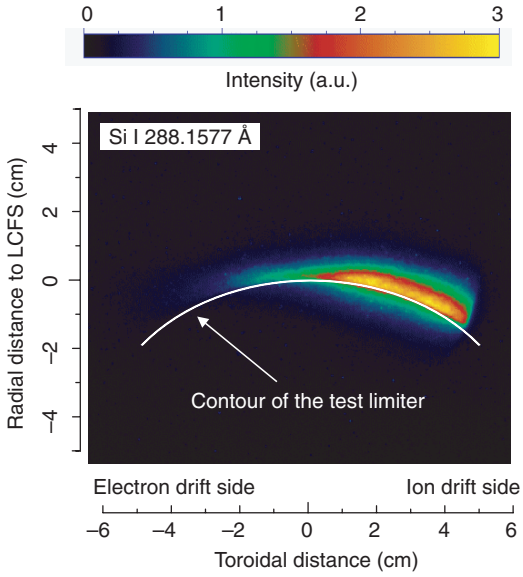

Figure 6. Spatial distribution of Si I-emission line above the test limiter coated with silicon layer ($y = 0$: LCFS, $y < 0$: scrape-off layer).

especially attractive to calculate the relative Si/D flux via $\Gamma(\mathrm{Si/D}) = I(\mathrm{Si\ II})/I(\mathrm{D}_\gamma) \times (S/XB(Si\ II))/(S/XB(\mathrm{D}_\gamma))$.

(b) Wavelength range 493–516 nm with Si II-emission lines at 504.1024 and 505.5984 nm corresponding to the transition $3s^2(^2P)4p$–$3s^2(^2D)4d$. The measured intensities of these lines normalized to the total intensity of the multiplet are 0.33 and 0.67 which is in a good agreement with theoretically predicted values [18] ($g_i A_{ik}/(g_i A_{ik} + g_j A_{jn})$, where g_i is the statistical weight of the level i and A_{ik} the transition probability from level i into k): 0.35 and 0.65.

(c) Wavelength range 584–605 nm with Si II-emission lines at 595.756 and 597.893 nm. These lines corresponds to the transition $3s^2(^2P)4p$–$3s^2(^2S)5s$. Due to He-beam diagnostic a strong overlap of observed spectral range with a He I-emission line (587.58 nm) was observed. Relative intensities of lines at 595.756 and 597.893 nm are 0.34 and 0.66 and match well with the theoretically predicted ones: 0.34 and 0.66

(d) Wavelength range 624–646 nm with Si II-emission lines at 634.711 and 637.137 nm corresponding to the transition $3s^2(^2S)4s$–$3s^2(^2P)4p$. Also in this spectral range the good correlation between predicted and measured relative intensities is observed: measured $I(634.711\ \mathrm{nm}) = 0.66$, $I(637.137\ \mathrm{nm}) = 0.34$ and the corresponding predicted relative intensities are 0.67 and 0.33.

These measurements were done with a spectrometer equipped with an intensified CCD camera as detector (resolution about 1 Å), which could be used for spatially (0.5 mm) and spectroscopically resolved measurements. Although this does not allow to resolve the splitting, the Zeeman effect may well have an influence on the line shape. However, for the presently observed lines—in emission—only the integral intensity is taken into account.

4.2. Experiments with injection of silane through test limiter

The measurements were made in series of Ohmic discharges with identical plasma parameters. Silane (SiD_4) gas was injected through the hole in the test limiter during the flat top phase

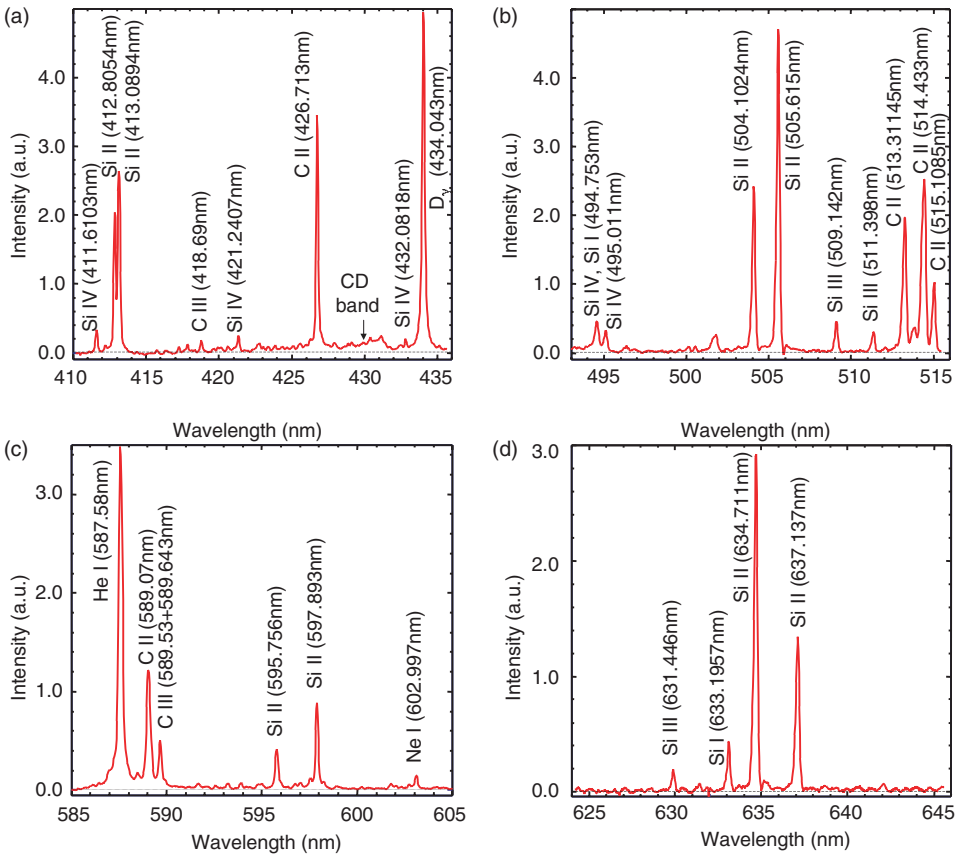

Figure 7. Typical Si II-emission spectra in front of test limiter.

(constant plasma current and density) of the discharges. The gas puff started after reaching the flat top phase of the discharges and the length of the gas puff was approximately 1 s. The local electron temperature was about 40 eV, the local electron density 2.0×10^{18} m^{-3} and the injection rate about 2.0×10^{18} SiD_4 molecules per discharge.

Figure 8 shows Si I-emission spectra in front of test limiter in three wavelength ranges:

(a) Wavelength range 245–265 nm with Si I-emission lines at 250.6897, 251.4316, 251.6112, 251.9202, 252.4108 and 252.8508 nm. These lines corresponds to the transition $3s^2 3p^2(^3P)$–$3s^2 3p4s(^3P)$. The measured relative intensities within the observed multiplet at 250.6897, 252.4108 and 252.8508 nm are 0.13, 0.14 and 0.17, that match the theoretically predicted ones well: 0.15, 0.12 and 0.15. Also the expected total intensity of lines at 251.4316, 251.6112, 251.9202 nm is 0.56, which is in good agreement to predicted ones: 0.58. Although, in the case of large injection rate (more than 10^{19} SiD_4) we observe strong deviation from theoretical ones: the expected total intensity of lines at 251.4316 and 251.6112 nm will be significantly smaller than theoretical value and the lines at 250.6897, 251.9202, 252.4108 and 252.8508 nm shows larger intensity values than predicted one. This can be explained due to the fact, that the emission lines at 251.4316 and 251.6112 nm with the largest oscillator strengths (0.157 and 0.115, respectively) and becomes optically thick in the case of large injection rate.

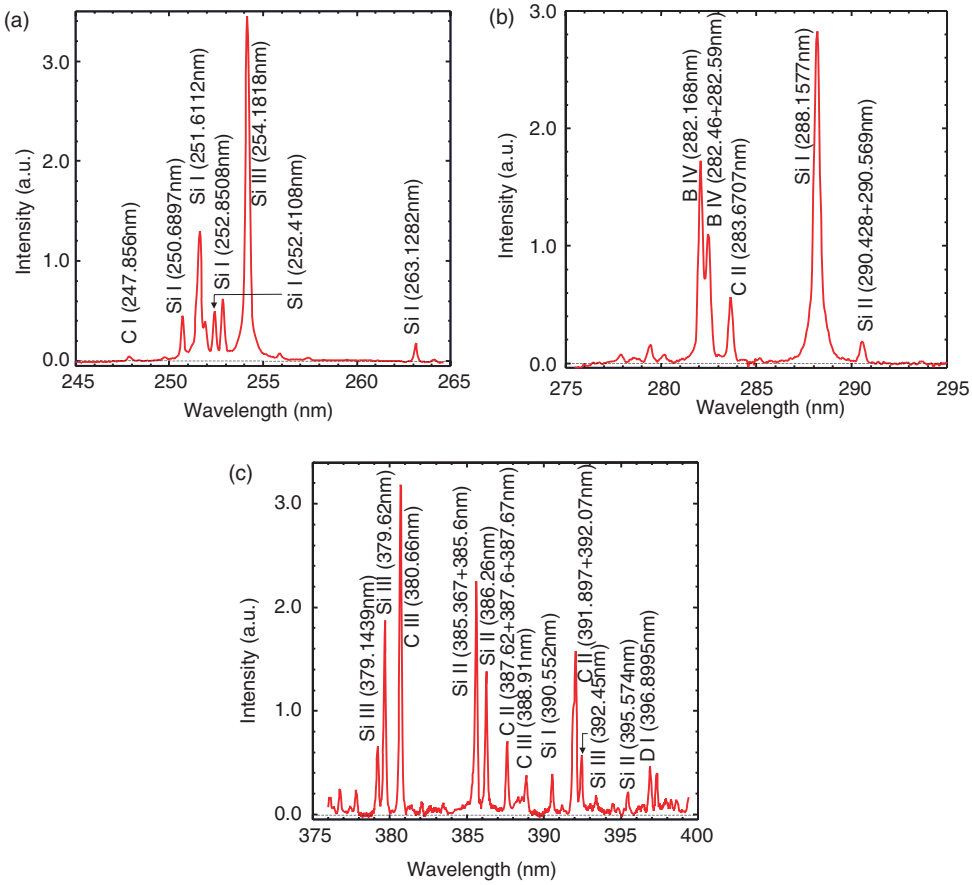

Figure 8. Typical Si I-emission spectra in front of test limiter.

(b) Wavelength range 275–295 nm with Si I-emission line at 288.1577 nm corresponding to the transition $3s^2 3p^2(^1D)$–$3s^2 3p4s(^1P)$. These measurements were made during the silane puff in fresh boronized TEXTOR, which display also some boron lines.

(c) Wavelength range 375–400 nm with Si I-emission lines at 390.552 nm (transition $3s^2 3p^2(^1S)$–$3s^2 3p4s(^1P)$).

Results from LIF on dissociated silane can be found in [30, 31] with due consideration of the Zeeman (Paschen-Back) effect. The corresponding temperatures of atomic silicon lie below 0.7 eV.

4.3. Comparison of experimental data with GKU kinetic code

As shown earlier, for lines with resolved fine structure, the relative intensities inside multiplets are in good agreement with the theoretical prediction. We consider below the sum over multiplet intensities, and the relative line intensities $r_\lambda = I(\lambda)/I(\lambda_0)$ with respect to the line $\lambda_0 = 412.9$ nm (3d–4f). Under assumption of identical silicon fluxes, it follows from equation (1) that $r_\lambda = I(\lambda)/I(\lambda_0) = S/XB(\lambda_0)/SXB(\lambda)$. Figure 9(*a*) shows the experimentally measured value r_λ and the calculated $S/XB(\lambda_0)/SXB(\lambda)$ for three different Si II-emission

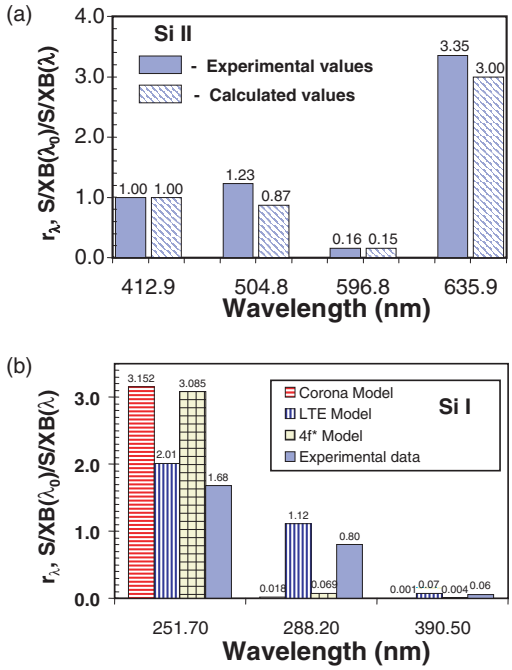

Figure 9. (*a*) Experimentally measured values $r_\lambda = I(\lambda)/I(\lambda_0)$ and calculated $S/XB(\lambda_0)/SXB(\lambda)$ for three different Si II-emission lines for a electron temperature $T_e = 40$ eV and a density $n_e = 2 \times 10^{18}\,m^{-3}$. (*b*) Comparison between the experimental (r_λ) and theoretical ($S/XB(\lambda_0)/SXB(\lambda)$) results with different model assumptions: corona, LTE and 4f*-models.

lines for electron temperature $T_e = 40$ eV and a local density $n_e = 2 \times 10^{12}\,cm^{-3}$. The measurements were performed in discharges with siliconized walls and identical plasma conditions. The measured intensities ratios $I(\lambda)/I(\lambda_0)$ for the three emission lines match the calculated data ($S/XB(\lambda_0)/SXB(\lambda)$) very well: the deviation between measured and calculated values for the emission lines at 596.8 nm (sum over multiplet lines 595.756 and 597.893 nm) and at 635.9 nm (sum over multiplet lines 634.711 and 637.137 nm) is smaller than 10% and for line 504.8 nm (sum over multiplet lines 504.1024 and 505.5984 nm) is about 29%.

Figure 9(*b*) shows a comparison between experimental and theoretical results with different model assumptions. At the radial position of the test limiter the T_e was about 40 eV and $n_e = 2.0 \times 10^{18}\,m^{-3}$. The experimental result is shown here as a ratio of line intensities $r_\lambda = I(\lambda)/I(\lambda_0)$ (normalized to the Si II-emission line at $\lambda_0 = 412.9$ nm) for Si I-emission lines at 251.7 nm (sum over multiplet lines 250.6897, 251.4316, 251.6112, 251.9202, 252.4108 and 252.8508 nm), 288.1577 nm and at 390.552 nm. The corresponding ratios ($S/XB(\lambda_0)/SXB(\lambda)$) were calculated by the GKU code with three different approaches:

(a) coronal approach with the assumption that only the ^3P term of the ground configuration $3p^2$ is populated;
(b) 'LTE' approach under the assumption of thermodynamic population (Boltzmann distribution) of the $3p^2$ SL terms (^3P, ^1D and ^1S);
(c) '4f*' is a coronal approach with the assumption of additional mixing through 4f states.

As can be seen in figure 9(*b*), the measured intensities ratios $I(\lambda)/I(\lambda_0)$ for the three emissions lines match the calculated with 'LTE' approach data ($S/XB(\lambda_0)/SXB(\lambda)$) very well: the

deviation between measured and calculated values for emission lines at 251.7 and 390.552 nm is smaller than 20% and for line 288.1577 nm is about 28%. Also the ratio between the Si I-emission lines $I(251.7\,\text{nm})/I(288.2\,\text{nm}) = 2.12$, $I(251.7\,\text{nm})/I(390.552\,\text{nm}) = 29.5$ correlates well with the calculated ones: 1.8 and 29, respectively. This indicates the applicability of the LTE-model only with significant population of metastable levels (^{1}D and ^{1}S) in the initial configuration of silicon atoms originating from the dissociation of the SiD_4 molecules. To prove the difference between physical sputtering and silane injection, the silicon fluxes were derived from Si II- (412.9 nm) and Si I-emission (288.2 nm) lines in the experiment with siliconized walls. The Si I line at 288.2 nm was chosen because this transition shows best the strong deviation between LTE and other models. The calculated fluxes from Si II (412.9 nm) and Si I (at 288.2 nm) show the same result (deviation lower than 30%), which demonstrates the applicability of LTE model with significant population of metastable levels (^{1}D and ^{1}S) in the initial configuration of silicon atoms for Si I-emission lines in the case of silicon release due to physical sputtering.

Corona and 4f* models result in a strong deviation at lines 288.2 and 390.552 nm: more than a factor of 50 for corona and about factor of 10 for the 4f*-model. If we use the LTE-model for calculation of *S/XB* ratios, all Si I- and Si II-emission lines observed in this paper provide identical silicon fluxes (the maximal deviation between fluxes are lower than 30%).

The absolute measured *S/XB*-values were obtained in the experiment with SiD_4 puffing under the assumption that one SiD_4 molecule provides one Si^+ ion and four deuterium atoms. In this case, the absolute *S/XB* ratios of Si II lines can be verified from the simultaneous increase of D_γ-emission and Si II-emission lines, caused by injected (dissociated) silane molecules: the *S/XB* value for D_γ-emission line is known (at $T_e = 40\,\text{eV}$, $n_e = 2 \times 10^{18}\,\text{m}^{-3}$ $S/XB = 300$ [33]). This is correct only under the formation of four deuterium atoms from silane because the possible formation of D_2 molecules can otherwise decrease the number of D_γ-photons per ionization event (*S/XB* ratio) [34]. Note that electron impact reactions with silane—the rates for electron impact reactions are given in [35, 36], the diverse rate coefficients are summarized in [37]—result in the formation of four deuterium atoms and one Si+ with probability of about 93.1% or in the formation of one D_2 molecule, two deuterium atoms and one Si+ with probability of about 6.9%. This obviously confirms our assumption about the formation of four deuterium atoms from silane in the range of experimental error.

Table 2 shows the comparison of measured *S/XB*-factors for Si II-emission lines (multiplets) and the predicted one for an electron temperature of 40 eV which are in agreement within 36%. Additionally, table 2 shows the experimental and calculated *S/XB* values for Si I at $T_e = 40\,\text{eV}$. Since the probability of the formation of Si^+ ion from silane is large, the procedure described above for Si II-emission lines is not applicable for neutral silicon, which is the reason why the measured rates were obtained by cross-calibration with Si II-emission lines. Again, the agreement between measured and calculated values is satisfactory.

Table 2. Comparison of measured absolute values of *S/XB* with theoretically predicted ones (GKU kinetic code) for $T_e = 40\,\text{eV}$ and $n_e = 2 \times 10^{18}\,\text{m}^{-3}$.

	Si II				Si I $3p^2$–3p4s		
	3d–4f 412.9 nm	4s–4p 635.9 nm	4p–5s 596.8 nm	4p–4d 504.8 nm	^{3}P–^{3}P 251.7 nm	^{1}D–^{1}P 288.16 nm	^{1}S–^{1}P 390.55 nm
S/XB values (GKU code)	14.5	4.95	90.0	16.5	7.2	13.0	210.0
S/XB values (experiment)	16.4	4.89	104.0	13.4	9.63	20.2	282.0

5. Conclusions

Measurements of Si I- and Si II-emission lines were performed in front of a test limiter under two different conditions: (i) silicon is sputtered from a silicon layer deposited on a graphite test limiter (ii) silane is puffed into the plasma through a gas inlet in the limiter head, releasing Si-atoms from the dissociation of the SiD_4 molecules.

It was shown that the relative intensities of the emission lines inside the multiplets are in good agreement with theoretical data calculated in the SL-coupling scheme. The values for *S/XB* were calculated using a collisional-radiative model (GKU kinetic code) in the electron temperature range below 100 eV for different electron densities and compared with the measured ones. The measured intensity ratios for Si II-emission lines are in reasonable agreement with calculated *S/XB* ratios within a maximum deviation of 30%. It was shown that the *S/XB* ratios depend strongly on electron temperature and that the dependence on electron density is weak. The measured values for Si I lines match the calculated ones if the populations of the $3p^2$ terms (^{3}P, ^{1}D and ^{1}S) are assumed to be in thermodynamical equilibrium (LTE). This indicates the significance of the population of metastable levels (^{1}D and ^{1}S) in the initial configuration of silicon atoms originating from the dissociation of the SiD_4 molecules. The successful applicability of the LTE model was shown in the case of silicon release due to physical sputtering.

For silicon flux measurements, the Si I-emission lines at 251.7 nm (transition $3p^2(^3P)$–$4s(^3P)$, sum over multiplet lines 250.6897, 251.4316, 251.6112, 251.9202, 252.4108 and 252.8508 nm) and 288.15 nm (transition $3p^2(^1D)$–$4s(^1P)$) should be the preferred choice. However, a disadvantage in the use of the Si I lines might lie in the accessibility in the UV region. In the case of Si II, the lines at 412.9 nm (transition 3d–4f, sum over multiplet lines 412.8054 and 413.0894 ,nm), 504.8 nm (transition 4p–4d, sum over multiplet lines 504.1024 nm and 505.5984 nm), and 635.9 nm (transition 4s–4p, sum over multiplet lines 634.711 and 637.137 nm) can be recommended for flux measurements. The flux values derived from Si I and Si II-emission lines using the calculated *S/XB* ratios are in agreement within 36%.

Acknowledgment

This work was supported in part (D Borodin, I Beigman and L Vainshtein) by RFBR (project 00-02-17825).

References

[1] Winter J *et al* 1993 *Phys. Rev. Lett.* **71** 1549
[2] Samm U *et al* 1995 *J. Nucl. Mater.* **220–222** 25
[3] Philipps V *et al* 2001 *J. Nucl. Mater.* **290–293** 1190
[4] Rapp J *et al* 2001 *J. Nucl. Mater.* **290–293** 1148
[5] Ongena J *et al* 1996 *Plasma Phys. Control. Fusion* **38** 279
[6] Philipps V *et al* 1994 *J. Nucl. Mater.* **212** (part B) 1189
[7] Roth J, Plank H and Schwörer R 1996 *Phys. Scr.* **T64** 67
[8] Plank H, Schwörer R and Roth J 1996 *Surf. Coat. Technol.* **83** 93
[9] Rocco P *et al* 1992 *J. Nucl. Mater.* **191–194** 474
[10] Behringer K H 1987 *J. Nucl. Mater.* **145–147** 145
[11] Pospieszczyk A 1993 Diagnostics of edge plasmas by optical methods *Atomic and Plasma Material Interaction Processes in Controlled Thermonuclear Fusion* ed R K Janev and H W Drawin (Amsterdam: Elsevier) p 21
[12] Behringer K *et al* 1989 *Plasma Phys. Control. Fusion* **31** 2059
[13] Philipps V *et al* 1998 *J. Nucl. Mater.* **258–263** 858
[14] Schweer B *et al* 1992 *J. Nucl. Mater.* **196–198** 174

[15] Beigman I L, Kocsis G, Pospieszczyk A and Vainshtein L A 1998 *Plasma Phys. Control. Fusion* **40** 1689
[16] Lebedev V S and Beigman I L 1998 *Physics of Highly Excited Atoms and Ions* (Berlin: Springer)
[17] Shevelko V P and Vainshtein L A 1993 *Atomic Physics for Hot Plasmas* (Bristol: Institute of Physics Publishing)
[18] Wiese W L, Smith M W and Miles B M 1969 *Atomic Transition Probabilities Vol II: Sodium Through Calcium NSRDS-NBS 22* (Washington, DC: NBS)
[19] Hey J D 1977 *J. Quant. Spectr. Radiat. Transfer* **18** 425
[20] Bell K L *et al* 1983 J. Phys. Chem. Rev. Data **12** 891
[21] Lennon M A *et al* 1988 *J. Phys. Chem. Rev. Data* **17** 1285
[22] Djuric N *et al* 1993 *Phys. Rev.* A **47** 478
[23] Freund R S, Wetzel R C, Shul R J and Hayes T R 1990 *Phys. Rev.* A **41** 3575
[24] Equipe T F R 1975 *Nucl. Fusion* **15** 1053
[25] Bogen P *et al* 1984 *J. Nucl. Mater.* **128–129** 157
[26] Stamp M F *et al* 1985 *Proc. 12th EPS Conf. On Controlled Fusion and Plasma Physics (Budapest, 1985)* vol 9F (part II) p 539
[27] Borodin D *et al* 2002 *Plasma Phys. Control. Fusion* **44** 2251
[28] van Regemorter H 1962 *Astrophys. J.* **136** 906
[29] Pospieszczyk A *et al* 1995 *Phys. Plasmas* **2** 2272
[30] Hey J D *et al* 2003 *16th Int. Conf. on Spectral Line Shapes AIP Conf. Proc.* vol 645 (New York: AIP) pp 26–39
[31] Mertens Ph and Silz M 1995 *7th Int. Symp. on Laser-Aided Plasma Diagnostics (Fukuoka, Japan)*
[32] Stull D R and Prophet H 1971 JANAF Thermochemical Tables NSRDS-NBS vol 37 National Bureau of Standards
[33] Summers H P 1994 *Atomic Data and Analysis Structure—User's Manual Report IR* (94) 06, JET Joint Undertaking, Abingdon and http://adas.phys.strath.ac.uk
[34] Pospieszczyk A *et al* 1999 *J. Nucl. Mater.* **266–269** 138
[35] Chatam H, Hills D, Robertson R and Gallagner A 1984 *J. Chem. Phys.* **81** 1770
[36] Perrin J, Schmitt J P M, de Rosny G, Drevillon B, Huc J and Lloret A 1982 *Chem. Phys.* **73** 383
[37] Kögler U and Winter J 1997 ERO-TEXTOR: 3D-Monte Carlo code for local impurity modelling in scrape-off-layer of TEXTOR *Report Jülich* Institut für Plasmaphysik, Jül-3361